Climbing the Bending Vibrational Ladder in $D^{13}C^{15}N$ by Hot Gas Emission Spectroscopy

Wolfgang Quapp,* Michael Hirsch,* Georg C. Mellau,† Stefan Klee,† M. Winnewisser,† and Arthur Maki‡

*Mathematisches Institut, Universität Leipzig, Augustus-Platz, D-04109 Leipzig, Germany; †Physikalisch-Chemisches Institut, Justus-Liebig-Universität Gießen, Heinrich-Buff-Ring 58, D-35392 Gießen, Germany; and ‡15012 24 Avenue S.E., Mill Creek, Washington 98012-5718

Using a newly constructed Fourier transform emission apparatus, we have measured the threefold substituted HCN isotopomer, $D^{13}C^{15}N$, at 1370 K in the range from 450 to 700 cm^{-1}. We could assign hot bands with upper states up to $v_2^l = 12^{12}$. The assignments have been verified for states up to $v_2 = 5$ by fitting with earlier room temperature absorption measurements of overtone and hot bands. The intensities are shown to be in qualitative agreement with the expected intensity pattern for such emission spectra. All the measurements for $D^{13}C^{15}N$ have been combined in a single least-squares fit that includes approximately 2700 rovibrational lines which have a root-mean-square deviation on the order of 0.000 4 cm^{-1}. The spectroscopic constants for the bending states $v_2 = 1, \ldots, 12$ are reported, as well as for some combination states involving the other vibrational modes. We also give the spectroscopic constants of various states of DCN, $D^{13}C^{14}N$, and $D^{12}C^{15}N$ which where obtained from room temperature absorption measurements. © 1999 Academic Press

INTRODUCTION

The spectrum of hydrogen cyanide, HCN, and that of its isotopomers has been measured extensively (*1–5*) because it is very simple and yet it shows many features that are of interest from a theoretical point of view. The spectrum is also the basis for comparison with ab initio calculations (*6–8*). The bending mode is of particular interest because of the large amplitude motion of the proton and also because the bending motion is a direct pathway to the isocyanide isomer, HNC. In earlier work Maki (*9*) showed that high-temperature absorption measurements on HCN can be used to observe transitions to quite high bending states. In another high-temperature study Maki and Sams (*10*) showed that absorption spectra of HNC could be obtained in equilibrium with HCN.

The linear $D^{13}C^{15}N$ molecule has three normal modes, two stretching vibrations of Σ^+ symmetry, and the bending mode of Π symmetry: ν_1 is the CD stretch at 2581.64 cm^{-1}, ν_3 is the CN stretch at 1885.32 cm^{-1}, and ν_2 is the degenerate bending mode at 560.07 cm^{-1}. [Some workers use a notation that reverses the role of ν_1 and ν_3 (*11*).] This is the first determination of the bending mode fundamental wavenumber of this isotopomer to our knowledge.

Prior to this work there seem to have been only three papers reporting measurements of this triply substituted species, $D^{13}C^{15}N$ (*12–14*); all were microwave or millimeter wave studies. The present work was undertaken to obtain further data for a systematic body of measurements giving an overview of the HCN potential energy surface and the pathway to isomerization. This surface has been studied by various theoretical methods (*8, 15*).

Using a newly constructed emission apparatus, we have studied the emission spectrum of the isotopically enriched

molecule $D^{13}C^{15}N$ at 1370 K (*16*). The Giessen Fourier transform spectrometer (FTS) was used in the range from 450 to 700 cm^{-1}. We also report room temperature absorption measurements of this and other isotopomers of DCN. The emission spectrum gives many transitions to previously unobserved bending states up to $v_2 = 12$ and some combinations of the CN stretch mode, ν_3, with various quanta of the bending mode, ν_2. Such high bending states can be observed because of the vibrational dependence of the harmonic oscillator transition moment, which has been described by Maki *et al.* (*3*).

Parallel to the analysis of the $D^{13}C^{15}N$ measurements, we have made similar analyses for DCN, $D^{13}C^{14}N$, and $D^{12}C^{15}N$. The data for the latter three isotopomers came from room temperature absorption measurements, some of which were not intentionally enriched in deuterium (*1–5*).

Recently Bernath reported on the progress in high-resolution Fourier transform emission spectroscopy (*17*). There exists only a small number of publications reporting the successful recording and analysis of high-resolution infrared emission spectra of polyatomic molecules in the gas phase. Most of the work has been done on diatomics, particularly on infrared electronic transitions of molecules involving transition elements. The reasons for supplementing our absorption studies on the HCN isotopomers by infrared emission were as follows: (i) to take advantage of the higher sensitivity and dynamic range of emission spectroscopy, which is in principle a zero-background method, (ii) to make accessible higher rovibrational states due to the substantial thermal excitation of the molecules at temperatures around 1370 K, and (iii) to induce partial isomerization to the presently not fully characterized species HNC and its isotopomers. Points (ii) and (iii) are strongly interconnected, since the bending vibration, which can

be thermally excited very efficiently, may be considered as the promoting mode for the isomerization process (*10*). In this measurement, we did not see the isomer D^{15}N^{13}C. Results concerning the emission spectroscopy of the HNC isomer will be reported elsewhere.

EXPERIMENTAL ASPECTS

All measurements were carried out in Giessen with a Bruker IFS 120 HR Fourier transform spectrometer. The individual HCN isotopomers were synthesized by treating isotopically labeled potassium cyanide (CIL, Andover, MA) with phosphorus pentoxide and H$_2$O and D$_2$O, respectively, as has been described elsewhere (*3*).

Emission Experiments

For emission spectroscopy, the spectrometer arrangement had to be modified compared with the setup for absorption experiments by moving the sample cell from the output port to the entrance aperture of the interferometer. An emission source cell was designed to optimize the signal-to-noise ratio for hot gas emission. The realization of this concept is shown to scale in Fig. 1. The main components of the emission experiment were the hot gas cell with cooled windows, an adjustable iris for limiting the radiative field of view, and an evacuated chamber with transfer optics that focused the infrared emission onto the entrance aperture of the spectrometer. Not shown in Fig. 1 is the additional evacuated detector chamber that was attached to the front exit of the parallel beam of the Bruker IFS120HR spectrometer. Inside that chamber a combination of two mirrors provided the focusing of the modulated radiation onto the detector aperture. The advantage of this setup in comparison to using the standard detection chamber was a minimal number of mirrors between emission cell and detector, thus reducing the radiation losses.

The emission cell was a one-m-long quartz tube with 5-cm inner diameter fitted with KBr windows that, together with their seals (Viton O-rings), were held at room temperature by a water-cooled collar at each end of the cell. The central part of the cell was enclosed in an electrically heated commercial furnace (RoK/A 6/60, Heraeus, Hanau, Germany) yielding a heated region of 60 cm in length at up to 1500 K. To avoid D/H exchange and thus keep the high isotopic purity of approximately 98% deuteration, the cell was treated several times with gaseous D$_2$O. Once the furnace and the preconditioned cell were at the required temperature, the cell was filled with the sample gas, D^{13}C^{15}N, to a pressure of 320 Pa, measured by a capacitance manometer (MKS baratron). For this pressure, the pressure-broadening contribution to the linewidth was ca. 0.002 cm^{-1}. Although a further increase in pressure would have brought a considerable increase in signal-to-noise ratio, this pressure was the upper limit where pressure broadening did not yet dominate the spectral linewidth and lineshift effects

could also be neglected. A larger contribution to the observed linewidth resulted from Doppler broadening, which was about 0.003 cm^{-1} full width at half maximum (FWHM) at wavenumbers around 600 cm^{-1}. The instrumental resolution was set at (maximum optical path difference)$^{-1}$ = 0.0050 cm^{-1}, which gives a FWHM of 0.003 cm^{-1}, just under the FWHM of the expected lines.

No indication of decomposition was found within the duration of the experiment of approximately 16 h (900 scans recorded at a scanner velocity of 1.27 cm/s). The spectral features remained constant during the entire data acquisition period. Unlike the stability found in these measurements with a quartz cell, an attempt to record hydrogen cyanide emission at further increased temperature in a ceramic cell failed, since it was found that HCN decomposes efficiently in such a cell.

To exploit the signal-to-noise ratio in principle attainable in emission, an adjustable iris kept at room temperature was introduced to limit the field of view of the interferometer to the central cylindrical volume of the emission cell. The aperture defined by this iris efficiently excluded the thermal continuum black body radiation of the cell walls from the modulated IR beam. A copper-doped germanium detector (Infrared Laboratories Inc., Tucson, AZ) was used that limited the radiation to wavenumbers in the range 400–900 cm^{-1}. It was used with a bandpass interference filter at liquid helium temperature inside the detector dewar. In practice, the room-temperature thermal background cannot be blocked, and therefore the single-beam spectra consisted of discrete D^{13}C^{15}N emission lines superposed on a modest thermal continuum. This situation turned out not to be a disadvantage, because on one hand the continuum could be removed by subtraction of an independently measured background spectrum from the sample spectrum, and on the other hand the continuum emission could be utilized to calculate the phase spectrum from the interferogram by the Mertz method, which requires spectral energy over the entire wavenumber interval within the detected range.

The rear window of the cell allowed the installation of a HeNe laser with an expanded beam for the precise alignment of the emission light path. In this way the combination of a spherical and a plane mirror in the transfer optics chamber could be carefully adjusted to image the emission perfectly on the entrance aperture and to align the input beam along the optical axis of the interferometer. With the experimental setup described and the parameters summarized in Table 1, a signal-to-noise ratio exceeding 1000 was achieved for the strongest emission lines.

The emission spectrum was calibrated by using the calibration factor determined for H^{12}C^{14}N emission lines against H^{12}C^{14}N lines from prior room temperature absorption spectra. The absolute accuracy of the emission linepositions is about ±0.0002 cm^{-1}. The absolute uncertainty of each band center can be estimated by taking the square root of the sum of the squares of the calibration uncertainty and the statistical uncertainty. Since the higher vibrational energy levels are determined by summing the band centers for several lower vibra-
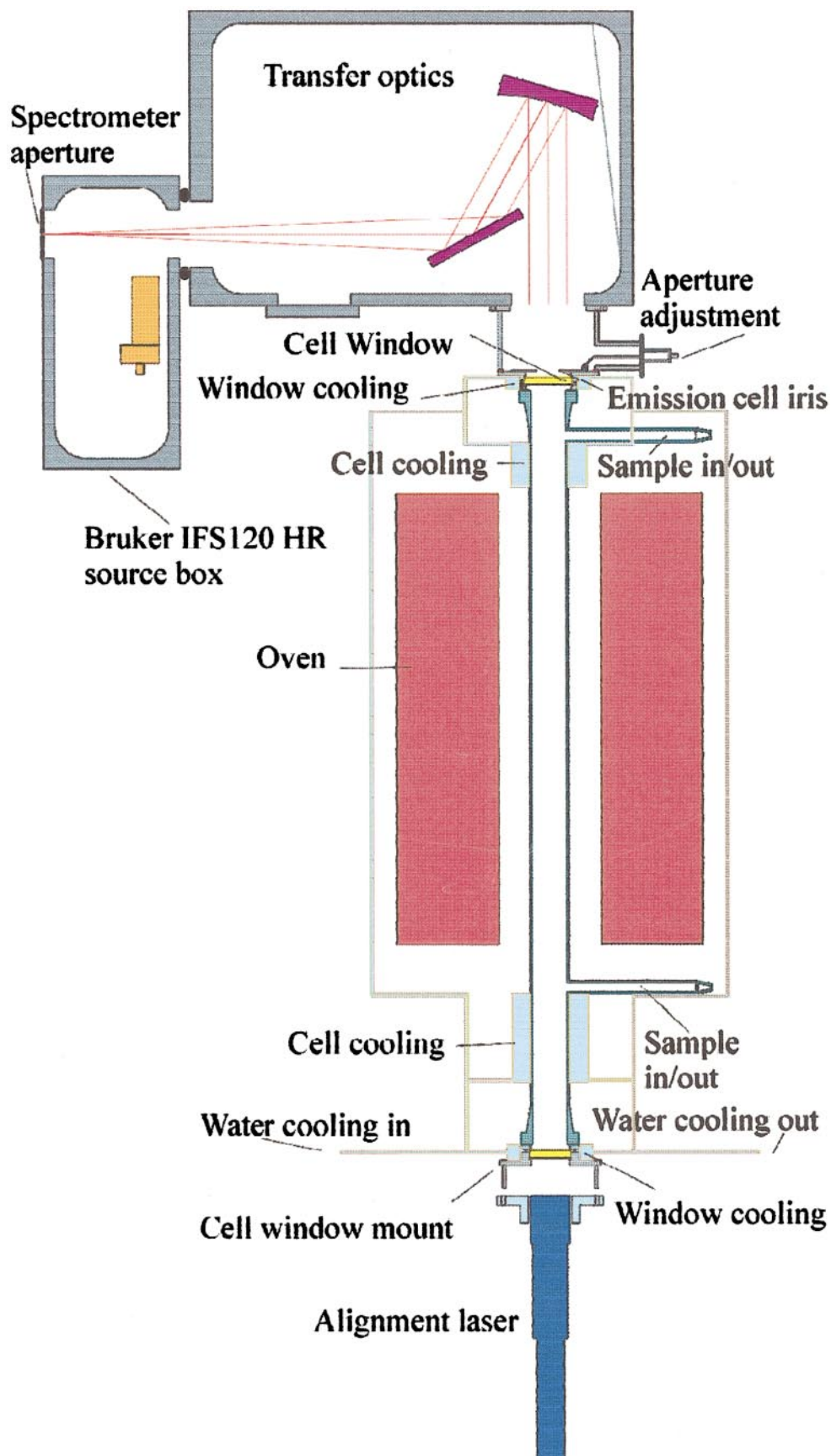
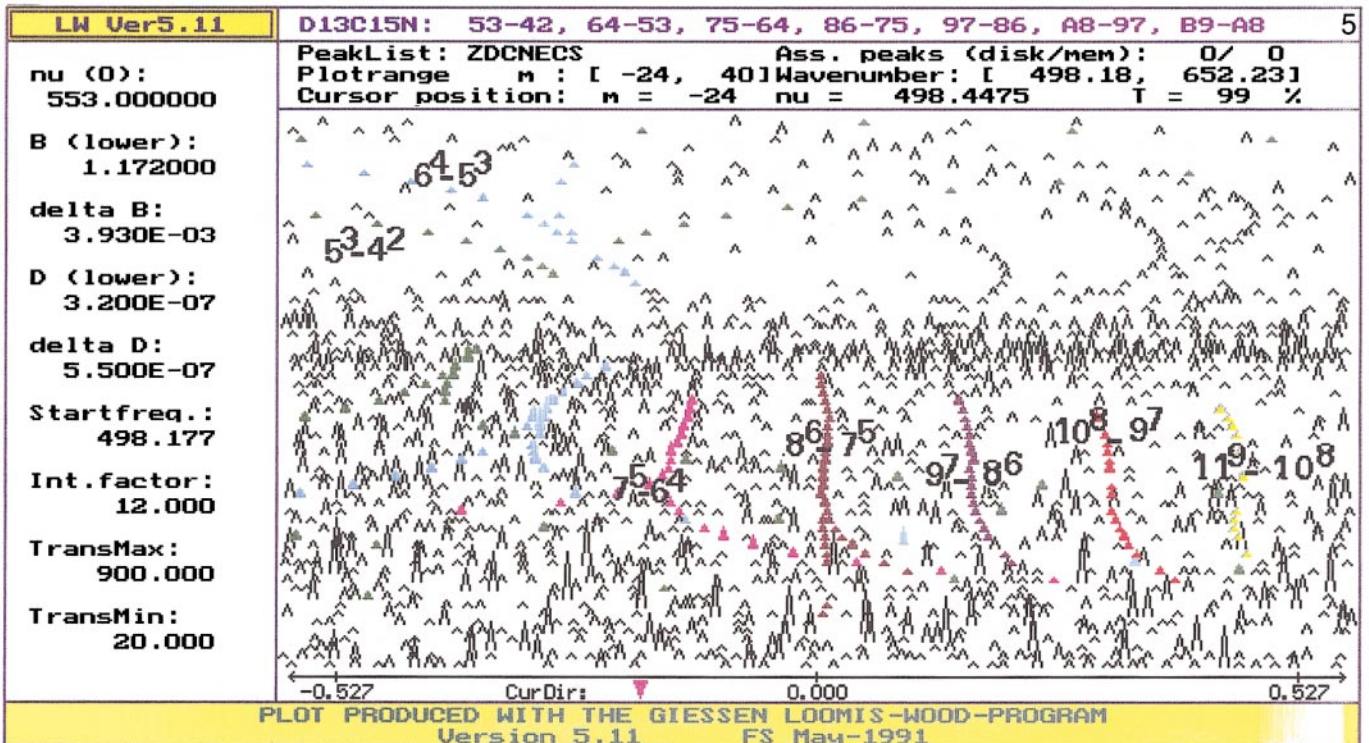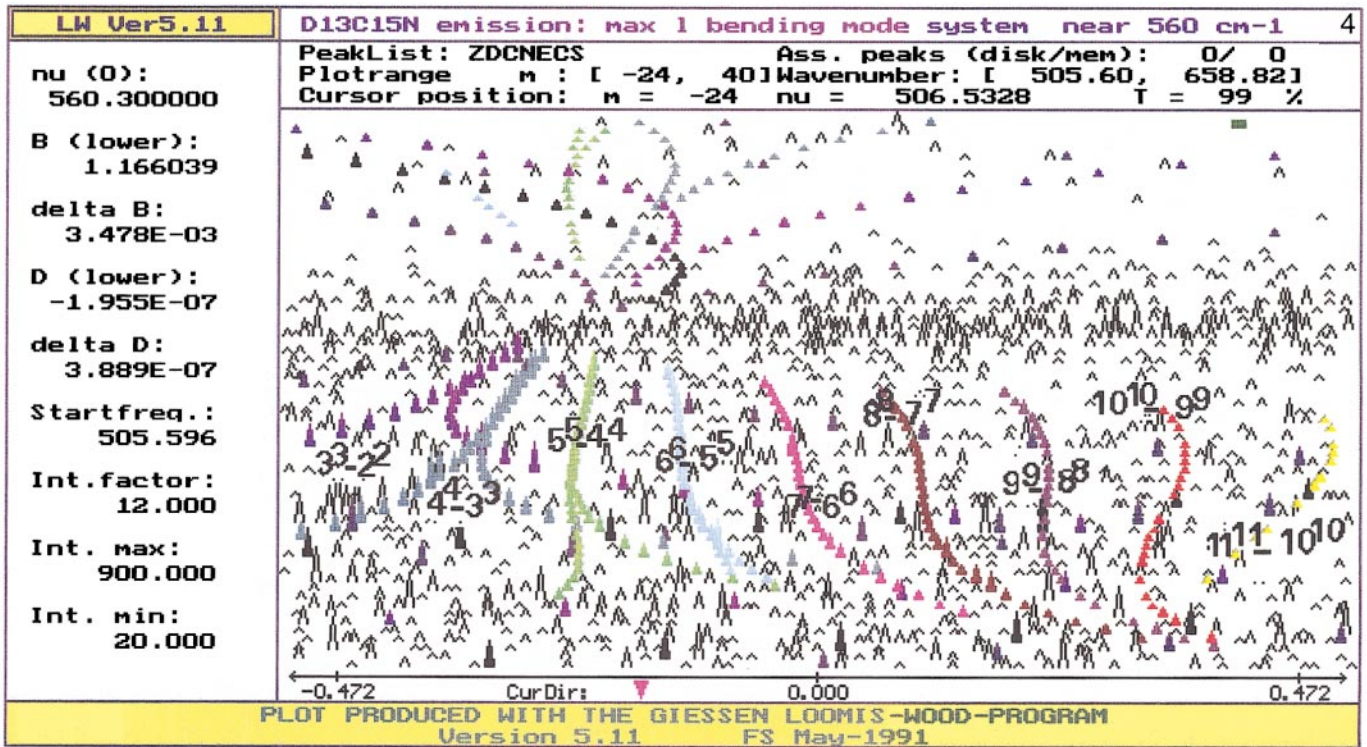**FIG. 1.**   Setup of the emission experiment.

FIG. 4. Loomis–Wood screen dump of the l_{max} transitions of the first 11 bending transitions of D¹³C¹⁵N of which the highest 10 are visible. The colors are as follows: $01^{1e}0\text{-}00^{0e}0$, black; $02^{2e,f}0\text{-}01^{1e,f}0$, brown-violet; $03^{3e,f}0\text{-}02^{2e,f}0$, violet; $04^{4e,f}0\text{-}03^{3e,f}0$, gray; $05^{5e,f}0\text{-}04^{4e,f}0$, green; $06^{6e,f}0\text{-}05^{5e,f}0$, light blue; $07^{7}0\text{-}06^{6}0$, pink; $08^{8}0\text{-}07^{7}0$, brown; $09^{9}0\text{-}08^{8}0$, dark violet; $010^{10}0\text{-}09^{9}0$, red; $011^{11}0\text{-}010^{10}0$, yellow.

FIG. 5. Loomis–Wood screen dump of the $l_{max}\text{-}2$ transitions of $05^{3e,f}0\text{-}04^{2e,f}0$ to $011^{9}0\text{-}010^{8}0$ of D¹³C¹⁵N. Colors are analogous to Fig. 4

TABLE 1
Parameters of FTS Spectral Measurements for $D^{13}C^{15}N$

Filename	EDCNECS	TGDCNFS	TGDCNGS	TGDCNHS
Type	Emission	Absorption	Absorption	Absorption
Region /cm^{-1}	400–877	900–1250	900–1250	900–1250
Date	4/2/1997	21/10/1995	23/10/1995	24/10/1995
Start pressure /mbar	3.2	0.266	2.62	2.31
End pressure /mbar		0.266	2.31	2.27
Temperature /K	1370	297	297	296
Pathlength /cm	60*	328	328	1968
Pressure×pathlength /cm mbar	192	87	853	4546
Aperture diameter /mm	3.15	1.5	1.5	1.5
Resolution (1/MOPD) /cm^{-1}	0.005	0.00222	0.00222	0.00222
Source		Globar	Globar	Globar
Bandpass opt. filter /cm^{-1}	400-900 (4K)	900-1300	900-1300	900-1300
High pass el. filter /cm^{-1}	194	829	829	829
Low pass el. filter /cm^{-1}	1026	1422	1422	1422
Scans coadded	680	450	350	450
Highest S/N (rms)	1000	300	300	300

* Heated region of the cell

For all measurements:

Detector	Ge:Cu (4K)
Windows (Detector and Cell)	KBr
Beamsplitter	Ge:KBr
Focal length of collimator /mm	418
Scanner velocity /cm/s	1.266

tional transitions, most of which come from the same spectrum with the same calibration, the error in the vibrational term values may be more accurately given by the product $\nu_2 \times (\pm 0.0002)$ cm^{-1}.

Absorption Experiments

For the absorption measurements of the HCN isotopomers we used a commercial White-type multipass absorption cell made of borosilicate glass (Infrared Analysis Inc., New York, NY). The cell had a base length of 0.82 m and a volume of approximately 7 liters. The optical pathlength was varied between four and 24 passes. Sample pressures were restricted to values below 500 Pa to avoid significant pressure-induced line broadening and shift effects. Absorption measurements were made on three isotopically enriched samples, $D^{12}C^{14}N$ from 400 to 1250 cm^{-1}, $D^{13}C^{14}N$ from 460 to 830 cm^{-1}, and $D^{13}C^{15}N$ from 900 to 1250 cm^{-1}. Bands outside those regions were either measured in the emission spectrum of $D^{13}C^{15}N$, or in absorption with samples containing $H^{12}C^{14}N$ or heavy-atom enriched samples of HCN.

For the calibration of the absorption spectra we used wavenumbers of H_2O present in the spectrum (18). Since the calibration constants were strongly dependent on the path-length adjustment of the multipass cell, each run had to be calibrated individually. The uncertainty of the absorption measurements due to calibration below and above 1500 cm^{-1} was determined to be ± 0.0002 and ± 0.0004 cm^{-1}, respectively.

ANALYSIS OF THE MEASUREMENTS

Assignment of the Transitions

In Fig. 2 we present an overview of the quite dense emission spectrum of the ν_2 region. The band center of the ν_2 fundamental of $D^{13}C^{15}N$ lies at 560.07 cm^{-1}. Note that the R-branch region is overlapped by P branches of the hot ν_2 transitions of $H^{13}C^{15}N$ with band center at 705.01 cm^{-1} (5). This impurity is caused by residual H_2O in the emission cell. Figure 3 shows some Q branches in the ν_2 region. The assignment of transitions was aided by the Giessen Loomis–Wood program (19). This program cuts the spectrum into segments of $2B$, where B is the rotational constant, and displays schematically consecutive segments, one above the other, on the monitor of a personal computer. With a good estimate of B'', and δB, lines belonging to a single subband will appear aligned in a recognizable pattern. A peculiarity of the $D^{13}C^{15}N$ isotopomer is a regular clustering in this presentation of the ladder of successive l_{max} hot bands of the bending mode. This is shown in Fig. 4, while Fig. 5 shows a similar pattern for the R-branch transitions of the $l_{max} - 2$ hot bands. The nearly parallel curves for the higher quantum numbers, beginning with $\nu_2 = 5$, make the assignment remarkably easy.

Estimated constants from previous data (12–14) or constants determined from a preliminary fit were useful in verifying the assignments. For spectra such as these, with a high density of
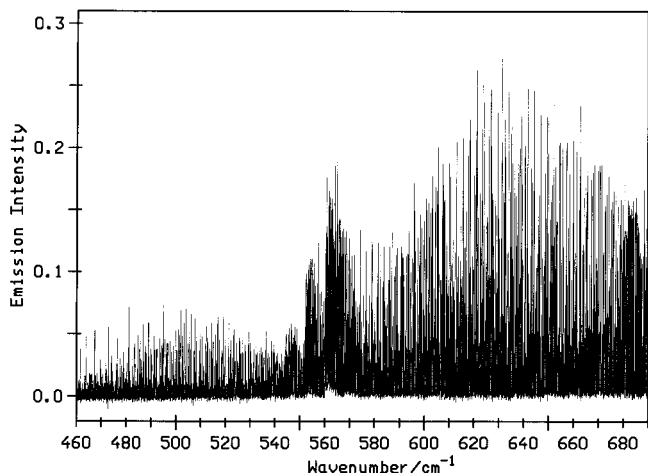
FIG. 2. Overview of the emission spectrum of the ν_2 region for D^{13}C^{15}N. The band center of the fundamental lies at 560 cm^{-1}. The R-branch region is badly overlapped by P-branch transitions of H^{13}C^{15}N.

lines, one must have a system for verifying new assignments based on predictions. Sometimes it seems we could assign any predicted transition because there is always a line near the predicted position! We have used several criteria for verifying our assignments: intensity, l-resonance splittings, rms deviation of the fit, and smooth variation of the rovibrational constants with vibrational quantum numbers.

From calculated intensities (see below) we know approximately how strong each transition should be. If a transition is too strong, it may be overlapped by another transition, but if it is too weak or is missing, then we must conclude that there is something wrong with our other assignments for the band in question. All transitions used in the fits had relative intensities that were in approximate agreement with the expected band intensity. No evidence was found for perturbations in the bands reported here for D^{13}C^{15}N.

In many cases the J and l assignments of D^{13}C^{15}N could be verified by the splitting of the e and f levels that can be resolved at sufficiently high J values. Even a crude approximation of the value of the l-type resonance constant will give an accurate estimate for the J value at which the splitting should first be observed for levels with $l > 1$. As a general rule, we have found that most of the transitions could be fit with an rms deviation of 0.0004 cm^{-1} or better. Weak transitions have somewhat larger rms deviations and some judgement had to be used to estimate what was an acceptable uncertainty for the weakest transitions. In many cases a given vibrational state was involved in more than one band. Our fitting procedure combines all the transitions involving a given state to obtain a single set of constants for that state.

Figure 6 gives an overview of the transitions found in emission for D^{13}C^{15}N. The observed transitions are shown by bold lines. In addition, we have measured the following transitions in absorption: 05^10–03^10, 05^30–03^30, 04^00–02^00,

04^20–02^20, 03^10–01^10, 03^30–01^10, 02^00–00^00, and 02^20–00^00. In Tables 2, 4, and 6 we give the largest J value, $J_{\max}$, that was included in the least-squares fit.

Vibrational and Rotational Constants

The constants obtained from the analysis of these measurements are given in Tables 2 and 3 for D^{13}C^{15}N and in Tables 4–6 for the other isotopomers. The present analysis is the same as that given in our earlier papers, but we give in the tables constants that are based on a more standardized notation. The observed transition wavenumbers, ν_{obs}, were fit with a nonlinear least-squares fitting program for which

$$\nu_{\text{obs}} = T(v, l, J)' - T(v, l, J)'', \qquad [1]$$

where the prime (′) and double prime (″) stand for the respective upper and lower state term values. The term values, $T(v, l, J)$, are given by the appropriate eigenvalues for the matrix formed with the diagonal matrix elements

$$\langle v_1, v_2, v_3, l, J | \mathbf{H}/hc | v_1, v_2, v_3, l, J \rangle$$
$$= G(v, l) + B_v[J(J+1) - l^2] \qquad [2]$$
$$- D_v[J(J+1) - l^2]^2 + H_v[J(J+1) - l^2]^3,$$

and with off-diagonal matrix elements

$$\langle v_1, v_2, v_3, l, J | \mathbf{H}/hc | v_1, v_2, v_3, l \pm 2, J \rangle$$
$$= \frac{1}{4}\{q_v - q_{vJ}J(J+1) + q_{vJJ}J^2(J+1)^2 + q_l(l \pm 1)^2\}$$
$$\times \{(v_2 \mp l)(v_2 \pm l + 2)[J(J+1) - l(l \pm 1)] \qquad [3]$$
$$\times [J(J+1) - (l \pm 1)(l \pm 2)]\}^{1/2}$$
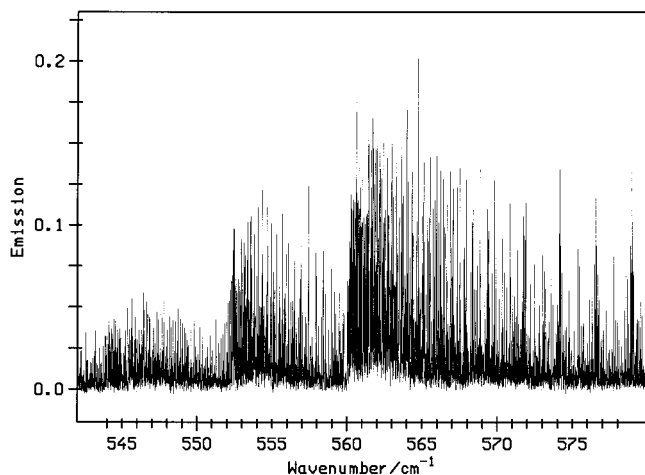
FIG. 3. Part of the emission spectrum with the Q branches in the ν_2 region of D^{13}C^{15}N. The clusters at the high frequency end are R branch lines at intervals of $2B$.
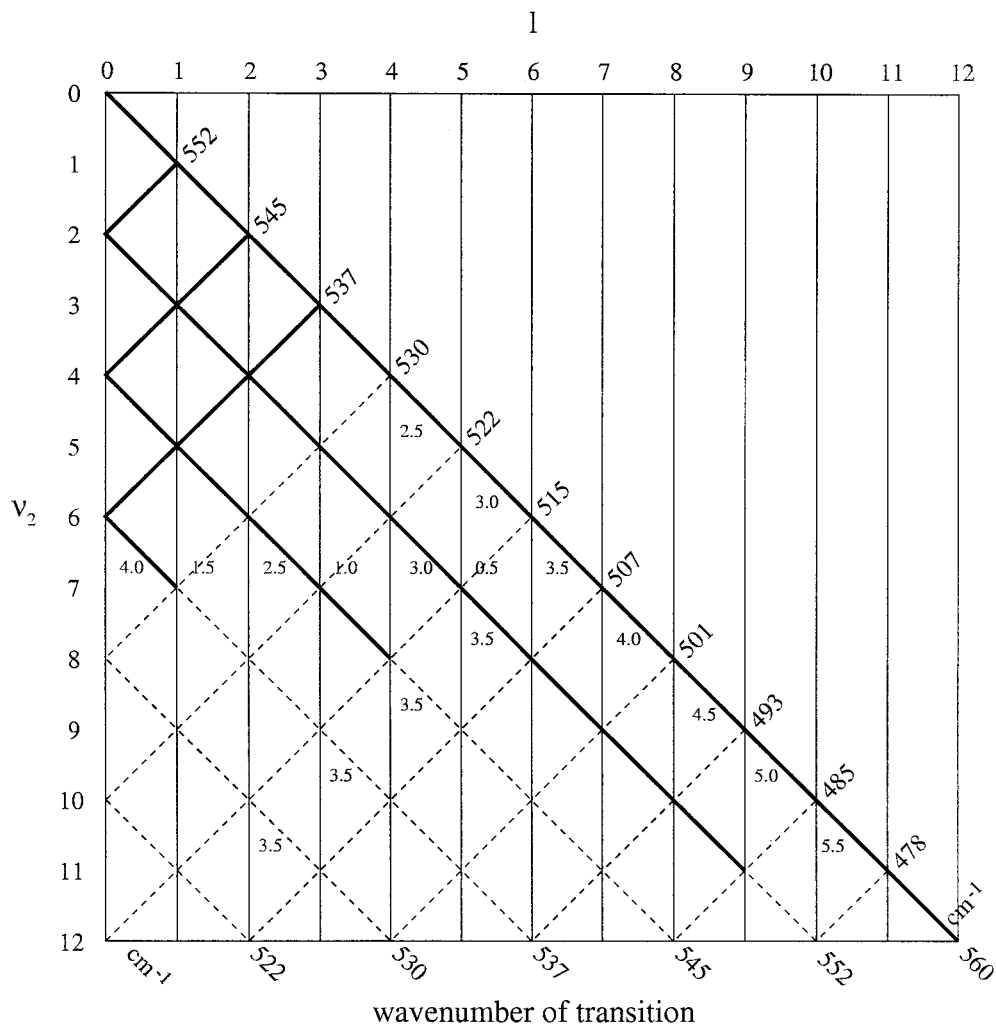
FIG. 6. Diagram of transitions in the ν_2 band system of $D^{13}C^{15}N$. The diagram is plotted as a matrix defined by ν_2 and l. Each grid point is a state, and the points are connected by diagonal lines representing transitions, where the bold lines are transitions observed in this work. Individual transitions along each of the consecutive sequences of diagonal lines cluster at nearly equal wavenumbers and the corresponding wavenumbers of the transitions from one grid point to the next are given at the end of each sequence. The positions of such clusters of bands are given along the lower axis for the $\Delta\nu = 1$, $\Delta l = 1$ series, and along the main diagonal for the $\Delta\nu = 1$, $\Delta l = -1$ series. (Loomis–Wood screen dumps of the transitions of the two sequences at the right are given in Figs. 4 and 5.) The small numbers within the grid, beside the lines for selected transitions, are the calculated L_ν scaling factors of the intensity of the corresponding transitions.

and

$$\langle \nu_1, \ \nu_2, \ \nu_3, \ l, \ J | \mathbf{H}/hc | \nu_1, \ \nu_2, \ \nu_3, \ l \pm 4, \ J \rangle$$

$$= \frac{1}{16} \, \rho_\nu \{ (\nu_2 \mp l)(\nu_2 \pm l + 2)(\nu_2 \mp l - 2)$$

$$\times (\nu_2 \pm l + 4)[J(J+1) - (l \pm 1)][J(J+1)$$

$$- (l \pm 1)(l \pm 2)][J(J+1) - (l \pm 2)(l \pm 3)]$$

$$\times [J(J+1) - (l \pm 3)(l \pm 4)]\}^{1/2}, \qquad [4]$$

where J is the quantum number for overall rotational angular momentum, l is the quantum number for vibrational angular momentum. The matrix has dimensions $(\nu_2 + 1) \times (\nu_2 + 1)$.

When $\nu_2 = 0$ this is a 1×1 matrix for which the term value, $T(\nu, l, J)$, is given by Eq. [2]. For vibrationally degenerated states the energy levels are divided into e and f levels defined according to their parity (20). For $D^{13}C^{15}N$ the e levels are below the f levels for all Π and Φ vibrational states, while for Δ and Γ states the f levels are below the e levels. We have arbitrarily assigned a positive sign to the q_ν constants, while the signs of the remaining terms in Eqs. [3] and [4] are then determined from the fit of the measurements.

The off-diagonal matrix elements given by Eqs. [3] and [4] represent the effect of l-type resonance, a type of Coriolis resonance. As long as there are no vibrational resonances, the usual definition of a vibrational transition, ν_0, is given by

$$\nu_0 = G(\nu, l)' - G(\nu, l)'', \qquad [5]$$

TABLE 2
Rovibrational Constants (in cm⁻¹) for D¹³C¹⁵N
after Correcting for l-type Resonance

v_1 v_2 l v_3	$G_0(v,l)^a$	B_v	$D_v \times 10^6$	$H_v \times 10^{12}$	J_{max}
0 0 0 0	0.0	1.151 840 202(64)^b	1.742 72(38)	1.88(15)	63
0 1 1 0	561.224 967(46)	1.155 674 022(49)	1.800 95(36)	2.45(14)	63
0 2 0 0	1112.434 443(48)	1.159 746 485(97)	1.864 44(47)	3.20(19)	47
0 2 2 0	1124.756 069(53)	1.159 389 167(70)	1.857 76(37)	3.02(14)	56
0 3 1 0	1666.060 453(51)	1.163 707 230(93)	1.927 30(52)	3.87(38)	47
0 3 3 0	1690.629 786(87)	1.162 975 465(147)	1.911 62(58)	3.54(34)	40
0 4 0 0	2209.868 915(96)	1.167 920 779(653)	1.995 75(81)	[4.54]^c	42
0 4 2 0	2222.126 442(85)	1.167 546 95(39)	1.987 45(38)	[4.37]	47
0 4 4 0	2258.880 957(185)	1.166 422 05(74)	1.962 39(67)	[3.87]	36
0 5 1 0	2756.192 606(184)	1.172 022 19(138)	2.062 55(191)	[5.16]	35
0 5 3 0	2780.654 579(213)	1.171 254 28(113)	2.044 22(117)	[4.83]	35
0 5 5 0	2829.542 772(234)	1.169 718 20(110)	2.009 37(111)	[4.16]	34
0 6 0 0	3292.828 716(467)	1.176 382 99(546)	2.148 7(107)	[5.87]	34
0 6 2 0	3305.042 402(606)	1.175 999 25(365)	2.134 22(531)	[5.71]	30
0 6 4 0	3341.665 588(365)	1.174 817 62(333)	2.087 82(710)	[5.22]	22
0 6 6 0	3402.646 212(413)	1.172 851 43(211)	2.048 85(264)	[4.37]	38
0 7 1 0	3832.032 494(760)	1.180 645 24(679)	2.185 7(127)	[6.50]	25
0 7 3 0	3856.424 20(106)	1.179 852 13(831)	2.222 4(160)	[6.17]	25
0 7 5 0	3905.179 269(527)	1.178 220 14(476)	2.129 28(896)	[5.50]	25
0 7 7 0	3978.220 102(483)	1.175 814 19(233)	2.094 30(271)	[4.49]	39
0 8 0 0	[4361.609 50]	[1.185 166 7]	[2.265 3]	[7.21]	
0 8 2 0	[4373.799 46]	[1.184 755 6]	[2.256 8]	[7.05]	
0 8 4 0	4410.349 61(128)	1.183 569 9(134)	2.316(35)	[6.54]	18
0 8 6 0	4471.214 17(121)	1.181 419 53(989)	2.058 7(156)	[5.70]	26
0 8 8 0	4556.291 023(633)	1.178 594 27(263)	2.136 03(222)	[4.53]	37
0 9 1 0	[4893.762 56]	[1.189 574 9]	[2.333 1]	[7.84]	
0 9 3 0	[4918.128 34]	[1.188 735 2]	[2.316 1]	[7.51]	
0 9 5 0	[4966.824 17]	[1.187 053 1]	[2.282 1]	[6.83]	
0 9 7 0	5039.780 77(131)	1.184 487 71(998)	2.117 8(146)	[5.83]	29
0 9 9 0	5136.883 907(749)	1.181 168 28(316)	2.161 72(261)	[4.49]	35
0 10 0 0	[5416.290 86]	[1.194 283 1]	[2.406 2]	[8.55]	
0 10 2 0	[5428.475 76]	[1.193 853 0]	[2.397 7]	[8.38]	
0 10 4 0	[5465.012 61]	[1.192 562 7]	[2.372 2]	[7.88]	
0 10 6 0	[5525.847 80]	[1.190 412 3]	[2.329 7]	[7.04]	
0 10 8 0	5610.891 79(231)	1.187 371 8(140)	2.173 6(170)	[5.87]	30
0 10 10 0	5720.020 20(123)	1.183 526 37(561)	2.177 54(466)	[4.36]	35
0 11 1 0	[5941.359 01]	[1.198 864 8]	[2.476 0]	[9.18]	
0 11 3 0	[5965.732 93]	[1.197 985 2]	[2.459 0]	[8.84]	
0 11 5 0	[6014.445 05]	[1.196 226 0]	[2.425 0]	[8.17]	
0 11 7 0	[6087.423 88]	[1.193 587 3]	[2.374 0]	[7.17]	
0 11 9 0	6184.559 94(247)	1.190 060 6(169)	2.243 4(237)	[5.83]	25
0 11 11 0	6305.718 51(140)	1.185 657 1(82)	2.184 4(106)	[4.15]	27
0 12 0 0	[6456.742 70]	[1.203 759 1]	[2.551 1]	[9.89]	
0 12 2 0	[6468.940 59]	[1.203 309 4]	[2.542 6]	[9.72]	
0 12 4 0	[6505.516 40]	[1.201 960 6]	[2.517 1]	[9.22]	
0 12 6 0	[6566.416 52]	[1.199 712 5]	[2.474 6]	[8.38]	
0 12 8 0	[6651.551 63]	[1.196 565 1]	[2.415 1]	[7.21]	
0 12 10 0	[6760.796 66]	[1.192 518 5]	[2.338 7]	[5.70]	
0 12 12 0	6893.988 20(349)	1.187 713 2(307)	2.839(60)	[3.85]	24
0 0 0 1	1885.322 912(77)	1.145 684 596(178)	1.741 00(112)	[1.89]	43
0 1 1 1	2448.577 456(273)	1.149 345 93(467)	1.804 24(103)	[2.45]	44
1 0 0 0	2581.635 472(128)	1.142 485 37(58)	1.726 61(48)	[1.89]	39
1 1 1 0	3128.150 374(690)	1.146 558 31(715)	1.777 7(154)	[2.45]	20

^{a} To get observed band center use $G_c(v,l) = G_0(v,l) - B_v l^2 - D_v l^4$.
^{b} The uncertainty in the last digits, twice the estimated standard error, is given in parentheses.
^{c} Constants enclosed in square brackets were fixed for the least-squares fit.

although ν_0 is not truly at the center of the band unless both the upper and lower states are $l = 0$ states. The true center of each band, ν_c, is given by

$$\nu_c = \nu_0 - B'_v l'^2 - D'_v l'^4 - H'_v l'^6$$
$$+ B''_v l''^2 + D''_v l''^4 + H''_v l''^6. \qquad [6]$$

The band centers, ν_c, for the bands measured in this work are given in Table 7. Some older papers such as Ref. (9) define ν_0 in such a way as to be the same as ν_c. Another convenient

notation is to define a term $G_0(v, l)$ relative to the zero-point energy

$$G_0(v, l) = G(v, l) - G(0, 0). \qquad [7]$$

These are the vibrational term values given in Tables 2, 4, and 6. The least-squares programs used to obtain the constants in Tables 2–10 are the same programs used for Refs. (1–5).

In only a few cases were all the higher order rovibrational constants adequately determined by the measurements. Rather

TABLE 3
l-type Resonance Constants
(in cm^{-1}) for D^{13}C^{15}N

$v_1\,v_2\,v_3$	$q_v \times 10^3$	$q_{vJ} \times 10^8$	$q_{vJJ} \times 10^{12}$
0 1 0	5.738 804 6(85)[a]	6.308 5(22)	1.105(16)
0 2 0	5.809 44(32)	6.646 1(409)	1.268(130)[b]
0 3 0	5.880 989(83)	6.962 2(240)	1.228(208)[b]
0 4 0	5.954 35(34)	7.267(62)	1.191(245)[c]
0 5 0	6.031 30(47)	7.848(68)	[1.33][d]
0 6 0	6.104 61(141)	8.331(248)	[1.39]
0 7 0	6.189 67(110)	8.429(248)	[1.44]
0 8 0	[6.269 7]	[8.71]	[1.50]
0 9 0	[6.353 2]	[9.05]	[1.55]
0 10 0	[6.438 5]	[9.40]	[1.61]
0 11 0	[6.525 8]	[9.74]	[1.67]
0 12 0	[6.614 9]	[10.08]	[1.72]
0 1 1	5.881 9(93)	[6.30]	[1.10]
1 1 0	5.615 58(162)	[6.30]	[1.10]

[a] The uncertainty in the last digits, twice the estimated standard error, is given in parentheses.
[b] Also fit was the $l,l\pm4$ coupling constant, $\rho = -0.506(\pm0.011)\times10^{-8}$ cm^{-1}.
[c] For $l>3$ the $l,l\pm4$ coupling constant was fixed at $\rho = -0.506\times10^{-8}$ cm^{-1}.
[d] Constants enclosed in square brackets were fixed for the least-squares fit.

than arbitrarily set to zero all those constants that could not be determined, we estimated the approximate value of the constants through the H_v, q_{vJJ}, and ρ_v terms. This was carried out by fitting the various constants to a power series in the vibrational quantum numbers as indicated later and extrapolating to estimate the values of those constants that could not be determined because the data were too sparse or too inaccurate. The analysis was done in several cycles. The first cycle determined which constants were determinable from the data. Those constants were then fit to a power series in order to calculate the undetermined constants for the next cycle. Some constants which could not be determined from the measurements were then held fixed at the calculated values in the next fit of the measurements. This gave improved values for the determinable constants and the cycle was repeated. This self-consistent procedure converged quite rapidly to give the constants reported in Tables 2–10.

Vibrational Quantum Number Expansions

The constants given in Tables 2–6 were fit to the usual power series expansion in the vibrational quantum numbers v and l to determine a set of constants which could be used to predict further rovibrational constants and unobserved term values. We have successfully used such predicted constants to climb up the bend-

TABLE 4
Rovibrational Constants in cm^{-1} for D^{12}C^{14}N
after Correcting for *l*-type Resonance

$v_1v_2l\,v_3$	$G_0(v,l)$[a]	B_v	$D_v \times 10^6$	$H_v \times 10^{12}$	J_{max}
0 0 0 0	0.0	1.207 750 949(14)[b]	1.927 17(25)	2.87(14)	45
0 1 1 0	570.252 867(17)	1.212 072 648(42)	1.997 09(26)	3.71(14)	46
0 2 0 0	1129.988 311(24)	1.216 649 433(91)	2.073 60(36)	4.92(22)	41
0 2 2 0	1142.756 669(21)	1.216 274 089(65)	2.065 18(29)	4.42(16)	40
0 3 1 0	1692.109 976(25)	1.221 113 899(80)	2.148 99(38)	6.02(28)	35
0 3 3 0	1717.545 949(48)	1.220 344 545(180)	2.130 43(65)	4.86(51)	34
0 4 0 0	2243.959 196(115)	1.225 850 042(1732)	2.233 0(31)	[7.12][c]	31
0 4 2 0	2256.637 108(262)	1.225 454 765(2102)	2.220 7(33)	[6.57]	28
0 4 4 0	2294.653 659(155)	1.224 270 495(1497)	2.189 2(28)	[4.94]	24
0 5 1 0	2798.308 931(343)	1.230 476 298(3955)	2.325 1(93)	[8.05]	23
0 5 3 0	2823.586 581(515)	1.229 663 504(5881)	2.291 4(147)	[6.96]	21
0 5 5 0	[2874.11]	[1.228 047]	[2.256]	[4.79]	
0 0 0 1	1925.255 513(89)	1.201 206 741(143)	1.925 76(40)	[2.83]	32
0 1 1 1	2498.340 939(211)	1.205 317 046(1893)	1.992 7(35)	[3.76]	26
1 0 0 0	2630.303 369(55)	1.197 414 795(274)	1.909 48(22)	[2.83]	37
0 2 0 1	3060.665(4)	1.209 723 1(318)	[2.072]	[4.97]	24
0 2 2 1	3073.474(5)	1.209 258 4(267)	[2.063]	[4.43]	22
1 1 1 0	3184.867 249(104)	1.202 028 402(551)	1.976 88(59)	[3.76]	36
0 3 1 1	3625.17(5)				
1 2 0 0	3729.134 851(415)	1.206 911 289(5138)	2.046 1(123)	[4.97]	21
1 2 2 0	3741.712 938(463)	1.206 589 587(5470)	2.044 7(123)	[4.43]	21
0 0 0 2	3836.35(5)	1.194 12(10)			
0 1 1 2	4412.175 3(14)	1.198 530 8(102)	2.000(15)	[3.76]	27
1 0 0 1	4523.275 158(239)	1.191 144 239(2061)	1.894 3(37)	[2.83]	32
1 1 1 1	5080.660(4)	1.195 688(48)	1.996(118)	[3.76]	19
2 0 0 0	5220.224 559(221)	1.187 048 007(1660)	1.897 74(231)	[2.83]	29
2 1 1 0	5759.049 631(2934)	1.191 960 86(4203)	2.003(128)	[3.76]	16

[a] To get observed band center use $G_c(v,l) = G_0(v,l) - B_v l^2 - D_v l^4$.
[b] The uncertainty in the last digits, twice the estimated standard error, is given in parentheses.
[c] Constants enclosed in square brackets were fixed for the least-squares fit.

TABLE 5
l-type Resonance Constants in cm^{-1} for
D^{12}C^{14}N, D^{13}C^{14}N, and D^{12}C^{15}N

$v_1v_2v_3$	$q_v \times 10^3$	$q_{vJ} \times 10^8$	$q_{vJJ} \times 10^{12}$
D^{12}C^{14}N			
0 1 0	6.210 659 4(9)[a]	7.347 5(11)	1.458(13)
0 2 0	6.288 350(53)	7.706 4(148)	1.539(95)[b]
0 3 0	6.368 304(25)	8.210 0(154)	2.439(137)[b]
0 4 0	6.449 99(89)	8.613(140)	[2.5][c,d]
0 5 0	6.534 35(16)	8.901(152)	[2.9][d]
0 1 1	6.391 15(225)	7.19(56)	[1.5]
0 2 1	6.548(37)	[7.76]	[1.8][d]
1 1 0	6.049 50(72)	8.541(97)	[1.5]
1 2 0	6.104 29(354)	[8.95]	[1.8][d]
0 1 2	6.662 8(62)	[7.35]	[1.5]
1 1 1	6.148 4(111)	[8.54]	[1.5]
2 1 0	5.900 58(927)	[9.74]	[1.5]
D^{13}C^{14}N			
0 1 0	6.080 680 4(99)	6.928 0(32)	1.262(29)
0 2 0	6.155 26(16)	7.251(16)	1.34(5)[e]
0 3 0	6.232 45(80)	7.675(198)	[1.60][e]
0 1 1	6.285 3(173)	[6.93]	[1.17]
1 1 0	5.911 93(314)	[6.93]	[1.17]
D^{12}C^{15}N			
0 1 0	5.873 430 6(33)	6.714 5(56)	1.17(19)
0 2 0	5.946 29(120)	[7.0]	[1.27][d]
0 3 0	6.021 31(25)	7.691(832)	[1.37][d]
0 1 1	6.019 06(891)	5.84(216)	[1.17]
1 1 0	5.746 95(444)	6.40(136)	[1.17]

[a] The uncertainty in the last digits, twice the estimated standard error, is given in parentheses.
[b] Also fit was the *l*,*l*±4 coupling constant, $\rho = -0.5652(\pm0.0022)\times10^{-8}$ cm^{-1}.
[c] Constants enclosed in square brackets were fixed for the least-squares fit.
[d] The *l*,*l*±4 coupling constant was fixed at the value $\rho = -0.5652\times10^{-8}$ cm^{-1}.
[e] Also fit was the *l*,*l*±4 coupling constant, $\rho = -0.5240(\pm0.0037)\times10^{-8}$ cm^{-1}.

ing vibrational ladder of D^{13}C^{15}N. The constants allowed us to calculate the emission lines for new vibrational transitions within an accuracy of ±0.05 cm^{-1} (10 line widths) or better when extrapolating to the next higher level. For the vibrational constants given in Table 8, we used the expansion

$$
G(v, l) = \sum_i^3 \omega_i(v_i + d_i/2) + \sum_{i \leq j}^3 x_{ij}(v_i + d_i/2)(v_j + d_j/2)
$$

$$
+ g_{22}l^2 + \sum_{i \leq j \leq k}^3 y_{ijk}(v_i + d_i/2)(v_j + d_j/2)
$$

$$
\times (v_k + d_k/2) + \sum_i^3 y_{ill}(v_i + d_i/2)l^2
$$

$$
+ \sum_{i \leq j \leq k \leq h}^3 z_{ijkh}(v_i + d_i/2)(v_j + d_j/2)
$$

$$
\times (v_k + d_k/2)(v_h + d_h/2) + \sum_{i \leq j}^3 z_{ijll}(v_i + d_i/2)
$$

$$
\times (v_j + d_j/2)l^2 + z_{llll}l^4 + z_{222ll}(v_2 + 1)^3 l^2
$$

$$
+ z_{22222}(v_2 + 1)^5. \tag{8}
$$

In this and the following equations the sums are over all values of the subscript from 1 to 3 for the three normal modes with $h \geq k \geq j \geq i$. The vibrational degeneracy is given by $d_1 = d_3 = 1$ and $d_2 = 2$.

Since the emission measurements for D^{13}C^{15}N go to very high bending states, it was necessary to include constants in Eq. [8] that involve high powers in the bending quantum number as well as high powers for the quantum number of the vibrational angular momentum, l. To make the constants comparable, the higher order terms were given the same values for the other isotopomers of DCN. In those cases where independent values can be obtained for all isotopomers, it can be seen in Table 8 that they only differ by a small amount. In those cases where a constant could not be determined for any isotopomer, it was necessary to set it to zero in the least-squares fit to Eq. [8]. All the x_{ij} constants could be determined only for D^{12}C^{14}N. Nakagawa and Morino (21) have given calculated values for those constants for D^{12}C^{14}N, D^{13}C^{14}N, and D^{12}C^{15}N and the ratios of those constants are very close to the ratios we observe. Consequently, we have used their calculated ratios to estimate the isotope shifts in those cases where the constants could not be determined from the measurements made at this time. Strey and Mills (22) have also given calculated values for the x_{ij} constants. Although they give fewer significant figures, their values are in fair agreement with those of Nakagawa and Morino.

The rotational constants are fit to

$$
B_v = B_e - \sum \alpha_i(v_i + d_i/2) + \sum \gamma_{ij}(v_i + d_i/2)(v_j + d_j/2)
$$

$$
+ \gamma_{ll}l^2 + \sum \gamma_{ijk}(v_i + d_i/2)(v_j + d_j/2)(v_k + d_k/2) \tag{9}
$$

$$
+ \sum \gamma_{ill}(v_i + d_i/2)l^2.
$$

The constants on the right side of Eq. [9] are given in Table 9. In several cases certain constants could be determined for some, but not all, isotopomers. In those cases the constants were set equal to the value found for another isotopomer. When a constant could not be determined for any isotopomer, it was set to zero. The centrifugal distortion constants given in Table 10 were calculated by

$$
D_v = D_e + \sum \beta_i(v_i + d_i/2) + \beta_{22}(v_2 + 1)^2 + \beta_{ll}l^2 \tag{10}
$$

and

$$
H_v = H^* + \xi_2(v_2 + 1) + \xi_{ll}l^2. \tag{11}
$$

Here the asterisk indicates that the constant is neither H_0 nor H_e. The corresponding constants for the stretching modes could not be estimated; they were set to zero. The *l*-type

TABLE 6
Rovibrational Constants in cm^{-1} for D^{13}C^{14}N and D^{12}C^{15}N
after Correcting for l-type Resonance

$v_1 v_2 l v_3$	$G_0(v,l)^a$	B_v	$D_v \times 10^6$	$H_v \times 10^{12}$	J_{max}
D^{13}C^{14}N:					
0 0 0 0	0.0	1.187 076 243(67)^b	1.855 35(56)	2.59(30)	40
0 1 1 0	562.524 814(22)	1.191 059 178(50)	1.918 45(54)	3.28(29)	41
0 2 0 0	1115.142 722(43)	1.195 292 756(106)	1.987 84(53)	4.33(27)	34
0 2 2 0	1127.321 242(40)	1.194 919 377(78)	1.979 45(53)	3.78(27)	36
0 3 1 0	1670.137 215(74)	1.199 411 074(816)	2.055 50(195)	[4.00]^c	24
0 3 3 0	1694.425 262(120)	1.198 645 271(1786)	2.036 84(293)	[4.00]	26
0 0 0 1	1911.841 518(48)	1.180 668 322(439)	1.856 35(74)	[2.90]	26
0 1 1 1	2476.332 17(327)	1.184 468 6(596)	2.060(218)	[3.50]	16
1 0 0 0	2590.066 802(184)	1.177 370 41(137)	1.838 71(180)	[2.90]	29
1 1 1 0	3137.755 68(115)	1.181 633 06(1191)	1.886 9(233)	[3.50]	21
D^{12}C^{15}N:					
0 0 0 0	0.0	1.173 138 248(3)	1.816 42(47)	[2.8]	34
0 1 1 0	568.971 927(27)	1.177 306 376(55)	1.881 93(67)	4.12(45)	33
0 2 0 0	1127.306 385(85)	1.181 717 265(75)	1.951 12(182)	[3.5]	28
0 2 2 0	1140.227 886(82)	1.181 357 834(87)	1.944 18(193)	[3.5]	21
0 3 1 0	X^d	1.186 019 173(215)	2.010 46(717)	[4.0]	
0 3 3 0	X + 25.657(68)	1.185 282 201(327)	2.010 46(717)	[4.0]	
0 0 0 1	1900.100 494(42)	1.166 849 756(141)	1.815 06(49)	[2.8]	35
0 1 1 1	2471.989 150(815)	1.170 833 94(750)	1.885 8(138)	[3.3]	27
1 0 0 0	2621.179 675(120)	1.163 162 559(755)	1.801 70(94)	[2.8]	31
1 1 1 0	3174.578 309(324)	1.167 591 52(407)	1.877 82(977)	[3.3]	20

^{a} To get observed band center use $G_c(v,l) = G_0(v,l) - B_v l^2 - D_v l^4$.
^{b} The uncertainty in the last digits, twice the estimated standard error, is given in parentheses.
^{c} Constants enclosed in square brackets were fixed for the least-squares fit.
^{d} Only rotational transitions have been observed for $3v_2$ of D^{12}C^{15}N.

resonance constants given in Tables 3 and 5 were fit to the equation

$$q_v = q_e + \sum \pi_i(v_i + d_i/2)$$
$$+ \sum \pi_{ij}(v_i + d_i/2)(v_j + d_j/2) \qquad [12]$$

to obtain the constants of q_v given in Table 10. The J-dependent terms are obtained from the expression

$$q_{vJ} = q_J^* + \pi_{1J}(v_2 + 1) + \pi_{2J}(v_2 + 1)^2. \qquad [13]$$

Table 10 gives the higher order constants only determined for the isotopomers D^{12}C^{14}N and D^{13}C^{15}N.

INTENSITIES

Aside from a frequency factor, the relative intensities of transitions in emission are much the same as the relative intensities of transitions in absorption. The absolute intensities are quite different, but in order to understand the form of the emission spectrum it is only necessary to consider the relative intensities. In emission the intensity of a given rovibrational transition, S_m, can be approximated by

$$S_m = 64\pi^4 \nu_m^3 L_v L_r \exp[-(E_r' + E_v')/kT]$$
$$\times 273.15 n A |\mu|^2/(3hQ_rQ_vTF), \qquad [14]$$

where Q_r and Q_v are the rotational and vibrational partition functions at the temperature of the measurement, n is Loschmidts number, E_r' and E_v' are the upper state rotational and vibrational energies, T is the temperature, F is the Herman–Wallis factor (assumed here to be 1.0), L_r is the usual Hönl–London rotational intensity factor, L_v is the vibrational intensity factor (2), A is the isotopic abundance of the species being considered, ν_m is the frequency of the line, and μ is the vibrational transition dipole moment. In Eq. [14] we have ignored the effects of self-absorption which are particularly important for understanding any quantitative intensity measurements because of the configuration of our sample cell, which has a layer of cool gas between the hot gas at the center of the cell and the cold windows.

Maki *et al.* (2) have shown that for molecules where Fermi resonance can usually be ignored, such as HCN, one can assume that all the hot bands for a given vibrational transition will have nearly the same transition dipole moment, μ_m. Then the most important terms that will be different for each emission line will be the Hönl–London term, L_r, the vibrational intensity factor, L_v, and the Boltzmann population of the emitting state. The frequency factor also becomes important at these low wavenumbers, but we shall ignore that factor for the time being. For the present case $\Delta v_2 = v_2' - v_2'' = 1$, therefore, the vibrational intensity term has the form

$$L_v = (v_2'' + l'' \Delta l + 2)/2g, \qquad [15]$$

TABLE 7
Band Centers in Wavenumbers (cm⁻¹) for the Infrared Bands
Measured in the Present Analysis

transition	ν_c	transition	ν_c	transition	ν_c
D¹³C¹⁵N		D¹³C¹⁴N		D¹²C¹⁴N	
01^10–00^00	560.069 293(46)*ᵃ	01^10–00^00	561.333 754(22)†	01^10–00^00	569.040 794(17)†
02^00–00^00	1112.434 443(48)†	02^00–00^00	1115.142 723(43)†	02^00–00^00	1129.988 311(24)†
02^20–00^00	1120.118 512(53)†	02^00–01^10	553.808 968(39)†	02^20–00^00	1137.891 573(21)†
02^00–01^10	552.365 150(50)*	02^20–01^10	561.207 810(34)†	02^00–01^10	560.947 517(19)†
02^20–01^10	560.049 219(50)*	03^10–02^00	553.795 082(68)†	02^20–01^10	568.850 778(15)†
03^10–01^10	1104.827 453(38)†	03^10–02^20	546.396 240(76)†	03^10–01^10	1121.848 068(20)†
03^30–01^10	1120.093 714(83)†	03^30–02^20	561.095 89(12)†	03^30–01^10	1137.522 054(46)†
03^10–02^00	552.462 303(48)*	04^00–03^10	546.474 59(25)†	03^10–02^00	560.900 551(20)†
03^10–02^20	544.778 234(54)*	04^20–03^10	553.780 08(30)†	03^10–02^20	552.997 290(20)†
03^30–02^20	560.044 495(77)*	04^40–03^30	560.998 10(29)†	03^30–02^20	568.671 275(44)†
04^00–02^00	1097.434 472(89)†	00^01–00^00	1911.841 518(48)†	04^00–02^00	1113.970 89(11)†
04^20–02^20	1097.337 743(77)†	01^11–01^10	1913.813 9(33)†	04^20–02^20	1113.843 72(27)†
04^00–03^10	544.972 168(88)*	10^00–00^00	2590.066 80(18)†	04^00–03^10	553.070 33(11)†
04^20–03^10	552.559 508(80)*	11^10–01^10	2575.240 3(12)†	04^20–03^10	560.846 43(27)†
04^20–03^30	537.293 25(10)*			04^40–03^30	568.502 48(16)†
04^40–03^30	560.055 20(17)*	D¹²C¹⁵N		05^10–03^10	1106.189 59(35)†
05^10–03^10	1090.123 84(18)†	01^10–00^00	567.794 620(27)†	05^30–03^30	1105.956 76(56)†
05^30–03^30	1089.950 28(22)†	02^00–00^00	1127.306 385(85)†	00^01–00^00	1925.255 513(89)†
05^10–04^00	545.151 67(17)*	02^00–01^10	559.511 764(84)†	01^11–00^00	2497.135 62(21)†
05^10–04^20	537.564 33(19)*	02^20–01^10	567.707 834(77)†	02^01–01^10	2491.624 6(39)†
05^30–04^20	552.657 04(21)*	00^01–00^00	1900.100 494(42)†	02^21–01^10	2499.596 5(49)†
05^50–04^40	560.081 61(17)*	01^11–01^10	1903.023 70(82)†	10^00–00^00	2630.303 369(55)†
06^00–05^10	537.808 13(43)*	10^00–00^00	2621.179 68(12)†	11^10–01^10	2614.624 43(10)†
06^20–05^10	545.317 82(59)*	11^10–01^10	2605.616 10(33)†	12^00–02^00	2599.146 54(41)†
06^40–05^30	552.755 22(34)*			12^20–02^20	2598.995 01(48)†
06^60–05^50	560.123 74(40)*			10^01–00^00	4523.275 16(24)†
07^10–06^00	538.023 13(68)*			20^00–00^00	5220.224 56(22)†
07^30–06^20	545.467 12(93)*			21^10–01^10	5188.816 9(30)†
07^50–06^40	552.855 26(45)*				
07^70–06^60	560.181 65(34)*				
08^40–07^30	545.606 97(84)*				
08^60–07^50	552.959 3(14)*				
08^80–07^70	560.255 78(53)*				
09^70–08^60	530.057 80(60)*				
09^90–08^80	560.348 29(53)*				
010^80–09^70	553.159 1(25)*				
$010^{10}0$–09^90	560.458 3(14)*				
011^90–010^80	553.265 0(16)*				
$011^{11}0$–$010^{10}0$	560.586 4(13)*				
$012^{12}0$–$011^{11}0$	560.703 5(73)*				
00^01–00^00	1885.322 912(77)†				
01^11–00^01	562.105 20(26)*				
10^00–00^00	2581.635 47(13)†				
11^10–01^10	2566.934 52(70)†				

ᵃ The uncertainty in the last digits (twice the standard deviation) is given in parentheses. An asterisk, *, indicates the band was measured in emission and a dagger, †, indicates the band was measured in absorption.

where $\Delta l = l' - l''$ and g is 2 unless either $l' = 0$ or $l'' = 0$. As an example of the significance of this term Table 11 shows the values of the L_v term for all the allowed transitions with $v_2'' = 6$. Except for the weakest three transitions at the bottom of the table, these transitions have been observed and the intensities are in rough agreement with Table 11 although we have not tried to make any quantitative intensity measurements.

The effects of the rotational Hönl–London term, L_r, are equally important. For P-branch transitions

$$L_r = \frac{1}{2}(|m| - l\Delta l - 1)(|m| - l\Delta l)/|m| \qquad [16]$$

and for R-branch transitions

$$L_r = \frac{1}{2}(|m| + l\Delta l + 1)(|m| + l\Delta l)/|m| \qquad [17]$$

where $|m| = (J' + J'' + 1)/2$, $l = l''$, and $\Delta l = l' - l''$. Table 11 also shows the value of these terms for $J' = 12$. These emission spectra have an intensity pattern that is equivalent to that of a perpendicular transition for a symmetric rotor. The intensity pattern resulting from the product $L_v L_r$ explains why we are able to observe high levels of v_2 only for the

TABLE 8

Constants (in cm^{-1}) for the Vibrational Energy Levels of Four Isotopomers of DCN

Parameter	D^{12}C^{14}N	D^{13}C^{14}N	D^{12}C^{15}N	D^{13}C^{15}N
ω_1	2702.545 05(518)[a]	2660.946 24	2693.572 47(56)	2652.570 51(79)
ω_2	579.747 93(838)	571.676 89	578.392 39(66)	570.306 39(73)
ω_3	1952.590 53(1946)	1938.912 18	1926.294 26(115)	1911.325 31(34)
x_{11}	-20.166 18(252)	[-20.438][b]	[-20.674]	[-20.879]
x_{22}	-2.159 80(273)	-1.982 929	-2.177 983(57)	-2.003 077(340)
x_{33}	-7.125 07(811)	[-7.083]	[-6.968]	[-6.928]
x_{12}	-15.780 64(517)	-14.926 93	-15.664 293(477)	-14.799 04(75)
x_{13}	-32.283 73(43)	[-30.181]	[-30.789]	[-28.784]
x_{23}	3.169 21(1619)	2.295 838	3.246 729(1143)	2.353 606(310)
g_{22}	3.261 508(259)	3.101 338	3.295 613(41)	3.137 391(110)
y_{222}	0.025 087(94)	0.020 940	[0.024]	0.021 055(90)
y_{112}	-0.024 91(249)	[-0.024]	[-0.024]	[-0.023]
y_{122}	0.063 01(32)	[0.062]	[0.062]	[0.060]
y_{223}	-0.112 22(539)	[-0.110]	[-0.110]	[-0.108]
y_{1ll}	-0.047 57(25)	[-0.047]	[-0.047]	[-0.045]
y_{2ll}	-0.017 434(115)	-0.013 157	[-0.016]	-0.013 451(54)
z_{2222}	-0.000 767 1(75)	[-0.000 72]	[-0.000 72]	-0.000 660 2(107)
z_{22ll}	0.000 795 0(146)	[0.000 75]	[0.000 75]	0.000 705 8(84)
z_{llll}	[-0.000 093]	[-0.000 093]	[-0.000 093]	-0.000 093 05(79)
z_{222ll}	[-0.000 004 3]	[-0.000 004 3]	[-0.000 004 3]	-0.000 004 31(44)
z_{22222}	[0.000 002 6]	[0.000 002 6]	[0.000 002 6]	0.000 002 62(48)
std. dev. of fit	3.3	--[c]	2.8	2.1
Number of non-zero weighted measurements:				
	25	9	8	33

[a] The uncertainty (one standard deviation) in the last digits is given in parentheses.
[b] Values enclosed in square brackets were fixed during the fit.
[c] For D^{13}C^{14}N the number of constants was equal to the number of measurements so all measurements are fit perfectly and no statistical analysis is possible.

highest possible l values, $l = v_2$. Of course, the density of lines and the signal/noise level precluded observing lines that were very weak.

As mentioned earlier the frequency factor can also be important for such long wavelength emission spectra. As an example, the highest wavenumber transition is near 690 cm^{-1}, and the lowest wavenumber transition used in our analysis is near 460 cm^{-1}. Just from the frequency factor alone the higher wavenumber transition would be stronger by a factor of $(690)^3/(460)^3 = 3.4$. In addition, the sensitivity of the spectrometer is lower at lower wavenumbers. Both these factors contribute to the obvious drop-off in intensity seen in the lower wavenumber region in Fig. 2. It also happens that the lower intensity $\Delta l = -1$ transitions occur in the lower wavenumber region.

TABLE 9

Rotational Constants (in cm^{-1} $\times$ 10^{-3}) for Four Isotopomers of DCN

Parameter	D^{12}C^{14}N	D^{13}C^{14}N	D^{12}C^{15}N	D^{13}C^{15}N
B_e	1211.900 14(766)	1191.184 31(1639)[a]	1177.127 57(384)	1155.776 42(926)
B_0	1207.750 949(22)	1187.076 236(36)	1173.138 248(3)	1151.840 210(133)
α_1	10.680 0(81)	10.032 53(659)	10.280 54(375)	9.632 97(1541)
α_2	-4.308 5(53)	-3.964 52(1637)	-4.157 89(379)	-3.833 12(921)
α_3	6.437 6(162)	6.323 3(321)	6.199 58(667)	6.073 14(1017)
γ_{11}	-0.015 31(136)	[-0.015][b]	[-0.014]	[-0.014]
γ_{22}	0.022 35(158)	0.021 300(47)	0.020 791(64)	0.019 221(266)
γ_{33}	-0.016 15(846)	[-0.016]	[-0.015]	[-0.015]
γ_{12}	0.217 05(1004)	0.206 69(646)	0.187 86(357)	0.166 13(1526)
γ_{13}	0.273 90(315)	[0.26]	[0.25]	[0.24]
γ_{23}	-0.211 25(292)	-0.182 65(3210)	-0.183 91(667)	-0.172 48(1015)
γ_{ll}	-0.093 65(148)	-0.092 896(127)	-0.089 774(163)	-0.089 534(199)
γ_{222}	0.000 570(49)	[0.000 5]	[0.000 5]	0.000 482 6(307)
γ_{122}	0.020 49(306)	[0.020]	[0.020]	[0.020]
γ_{1ll}	0.013 40(292)	[0.013]	[0.013]	[0.013]
γ_{2ll}	-0.002 241(53)	-0.002 264(39)	-0.002 143(50)	-0.002 043(67)
z_{22ll}	[-0.000 017]	[-0.000 017]	[-0.000 017]	-0.000 017 2(49)
std. dev. of fit:	3.1	1.1	1.8	4.2
number of non-zero weighted measurements:				
	25	10	10	34

[a] The uncertainty (one standard deviation) in the last digits is given in parentheses.
[b] Values enclosed in square brackets were fixed during the fit.

CONCLUSION

The constants given in Tables 8–10 are in good agreement with those given by the force field calculations of Nakagawa and Morino (*21*) and Strey and Mills (*22*). In addition, the vibrational dependence of D and q and the ratio of their values for the different isotopomers are in good agreement with the predictions of Nakagawa and Morino (*23*). The current best estimate of the value for B_e for D^{12}C^{14}N, 36 331.85 ± 0.23 MHz, is well within twice the standard deviation of the earlier value given by Winnewisser *et al.* (*24*), 36 329.49 ± 1.53 MHz.

It is interesting to note that the bending vibration is not very anharmonic since 10 constants are enough to fit fairly well the 29 observed bending levels that extend up to $v_2 = 12$. It was found earlier that one almost needed a new constant to fit each measurement of a new stretching state for HCN.

For the first time these measurements show that the band

TABLE 10
Some Higher Order Constants in cm^{-1}

Parameter	D^{12}C^{14}N	D^{13}C^{15}N
$D_e \times 10^6$	1.865 79(129)[a]	1.686 19(253)
$\beta_1 \times 10^7$	-0.151(12)	-0.125(21)
$\beta_2 \times 10^7$	0.698(11)	0.617(12)
$\beta_3 \times 10^7$	-0.016(7)	0.013(29)
$\beta_{22} \times 10^7$	0.012 3(17)	0.005 0(20)
$\beta_{12} \times 10^7$	-0.025 7(95)	[-0.024]
$\beta_{ll} \times 10^7$	-0.022 8(10)	-0.021 3(12)
std. dev.	2.9	7.4
# of measurements	22	34
$H^* \times 10^{12}$	2.83(5)	1.853(29)
$\xi_2 \times 10^{12}$	1.072(37)	0.669(23)
$\xi_{ll} \times 10^{12}$	-0.136(19)	-0.042(10)
std. dev.	0.8	0.4
# of measurements	6	6
$q_e \times 10^3$	6.126 2(363)	5.665 8(95)
$\pi_1 \times 10^4$	-0.87(13)	-0.492(33)
$\pi_2 \times 10^4$	0.444(178)	0.383 8(47)
$\pi_3 \times 10^4$	-0.28(72)	-0.59(18)
$\pi_{11} \times 10^4$	0.061(46)	[0.060][b]
$\pi_{22} \times 10^4$	0.010 61(19)	0.009 51(72)
$\pi_{33} \times 10^4$	0.456(37)	[0.44]
$\pi_{12} \times 10^4$	-0.230(36)	[-0.23]
$\pi_{13} \times 10^4$	-0.82(11)	[-0.80]
$\pi_{23} \times 10^4$	0.79(35)	[0.77]
std. dev.	2.0	4.1
# of measurements	12	9
$q_J^* \times 10^8$	6.934(16)	5.965(13)
$\pi_{1J} \times 10^8$	1.19(22)	[0.0]
$\pi_{2J} \times 10^8$	0.413(15)	0.343(12)
std. dev.	4.5	2.9
# of measurements	7	7

[a] The uncertainty in the last digits, one standard deviation, is given in parentheses.
[b] Constants enclosed in square brackets were fixed for the least-squares fit.

TABLE 11
Vibrational and Rotational Intensity Factors

transition	L_v	$L_r P(13)$	$L_r R(11)$
07^{7}0–06^{6}0	3.5	1.615	14.250
07^{5}0–06^{4}0	3.0	2.769	11.333
07^{3}0–06^{2}0	2.5	4.231	8.750
07^{1}0–06^{0}0	4.0	6.000	6.500
07^{1}0–06^{2}0	1.5	8.077	4.583
07^{3}0–06^{4}0	1.0	10.462	3.000
07^{5}0–06^{6}0	0.5	13.154	1.750

center, ν_c, of the bending fundamental of D^{13}C^{15}N is at 560.07 cm^{-1}. This work also demonstrates that emission measurements can be used to explore the ladder of bending vibrational states up to term values of 6700 cm^{-1}, much higher than the ground state of the isocyanide isomer, DNC. Our new constants could also be used to improve by over an order of magnitude the transition wavenumbers derived by Thanh and Rossi (*25*) from literature constants for DCN. Because of the many new measurements on the deuterated isotopomers, we can confirm the assignments of the millimeter wave spectrum given for all four DCN isotopomers for $v_2 \leq 3$ by Preusser and Maki (*14*). Their measurements as well as all other available data were included in our fit. All of the data of D^{13}C^{15}N that were used in our fits are available as an addendum to this paper.[1]

REFERENCES

1. W. Quapp, S. Klee, G. C. Mellau, S. Albert, and A. Maki, *J. Mol. Spectrosc.* **167,** 375–382 (1994).
2. A. Maki, W. Quapp, and S. Klee, *J. Mol. Spectrosc.* **171,** 420–434 (1995).
3. A. Maki, W. Quapp, S. Klee, G. C. Mellau, and S. Albert, *J. Mol. Spectrosc.* **174,** 365–378 (1995).
4. A. Maki, W. Quapp, S. Klee, G. C. Mellau, and S. Albert, *J. Mol. Spectrosc.* **180,** 323–336 (1996).
5. A. Maki, W. Quapp, S. Klee, G. C. Mellau, and S. Albert, *J. Mol. Spectrosc.* **185,** 356–369 (1997).
6. P. Botschwina, B. Schulz, M. Horn, M. Matuschewski, *Chem. Phys.* **190,** 345–362 (1995).
7. P. Botschwina, M. Horn, M. Matuschewski, E. Schick, and P. Sebald, *J. Mol. Struct.* **400,** 119–137 (1997).
8. A. J. C. Varandas, and S. P. J. Rodrigues, *J. Chem. Phys.* **106,** 9647–9658 (1997).
9. A. G. Maki, *J. Mol. Spectrosc.* **58,** 308–315 (1975).

10. A. G. Maki and R. L. Sams, *J. Chem. Phys.* **75,** 4178–4182 (1981).

11. A. M. Smith, S. L. Coy, W. Klemperer, and K. K. Lehmann, *J. Mol. Spectrosc.* **134,** 134–153 (1989).

12. E. F. Pearson, R. A. Creswell, M. Winnewisser, and G. Winnewisser, *Z. Naturforsch.* **31a,** 1394–1397 (1976).

13. M. Winnewisser and J. Voigt, *Z. Naturforsch.* **33a,** 1323–1327 (1978).

14. J. Preusser and A. G. Maki, *J. Mol. Spectrosc.* **162,** 484–497 (1993).

15. J. M. Bowman, B. Gazdy, J. A. Bently, T. J. Lee, and C. E. Dateo, *J. Chem. Phys.* **99,** 308–323 (1993).

16. G. C. Mellau, and M. Winnewisser, *"15th Colloquium on High Resolution Spectroscopy,"* M3, Glasgow 1997.

17. P. F. Bernath, *Chem. Soc. Rev.* **25,** 111–115 (1996).

18. G. Guelachvili and K. Narahari Rao, "Handbook of Infrared Standards," Academic Press, London, UK (1986).

19. B. P. Winnewisser, J. Reinstädtler, K. M. T. Yamada, and J. Behrend, *J. Mol. Spectrosc.* **136,** 12–16 (1989); F. Stroh, J. Reinstädtler, J. C. Grecu, and S. Albert, "The Giessen Loomis-Wood Program LW 5.1" Justus-Liebig-Universität Giessen, 1992.

20. J. M. Brown, J. T. Hougen, K.-P. Huber, J. W. C. Johns, I. Kopp, H. Lefebvre-Brion, A. J. Merer, D. A. Ramsay, J. Rostas, and R. N. Zare, *J. Mol. Spectrosc.* **55,** 500–503 (1975).

21. T. Nakagawa and Y. Morino, *J. Chem. Soc. Japan* **42,** 2212–2219 (1969).

22. G. Strey and I. M. Mills, *Mol. Phys.* **26,** 129–138 (1973).

23. T. Nakagawa and Y. Morino, *J. Mol. Spectrosc.* **31,** 208–229 (1969).

24. G. Winnewisser, A. G. Maki, and D. R. Johnson, *J. Mol. Spectrosc.* **39,** 149–158 (1971).

25. N. V. Thanh and I. Rossi, *J. Mol. Spectrosc.* **148,** 160–179 (1991).